

Review

Time Reversal Symmetry Breaking Superconductors: Sr_2RuO_4 and Beyond

Karol Izydor Wysokiński 

Institute of Physics, M. Curie-Skłodowska University, ul. Radziszewskiego 10, 20-031 Lublin, Poland;
karol@tytan.umcs.lublin.pl

Received: 9 March 2019; Accepted: 6 May 2019; Published: 9 May 2019



Abstract: Recent work done on the time reversal symmetry (TRS) breaking superconductors is reviewed in this paper. The special attention is paid to Sr_2RuO_4 believed to be spin triplet chiral p-wave superconductor which break TRS and is expected to possess non-trivial topological properties. The family of TRS breaking superconductors is growing relatively fast, with many of its newly discovered members being non-centrosymmetric. However not only Sr_2RuO_4 but also many other superconductors which possess center of inversion also break TRS. The TRS is often identified by means of the muon spin relaxation (μSR) and the Kerr effect. Both methods effectively measure the appearance of the spontaneous bulk magnetic field below superconducting transition temperature. This compound provides an example of the material whose many band, multi-condensate modeling has enjoyed a number of successes, but the full understanding has not been achieved yet. We discuss in some details the properties of the material. Among them is the Kerr effect and by understanding has resulted in the discovery of the novel mechanism of the phenomenon. The mechanism is universal and thus applicable to all systems with multi-orbital character of states at the Fermi energy.

Keywords: time reversal symmetry breaking; spin triplet superconductivity; chiral order parameter; polar Kerr effect

1. Introduction

Discovery of the high-temperature superconductors [1] a few decades ago has started a vivid and still ongoing experimental and theoretical race to uncover their secrets. This breakthrough in the research of superconductivity was preceded by the discovery of CeCu_2Si_2 , the first heavy fermion superconductor [2] and other members of this family UBe_{13} [3] and UPt_3 [4]. The concomitant development of the new technologies of the material synthesis, and the curiosity these findings have evoked, resulted in the numerous discoveries of simple, like MgB_2 [5], and more complex families of the superconducting materials including Sr_2RuO_4 [6] the perovskite superconductor without copper.

Very recently, excitement has stimulated the discovery of systems superconducting at high pressures. These findings culminated in measurements of the superconducting materials with transition temperatures T_c approaching the freezing temperature of water [7,8]. Novel superconductors are often denoted as exotic [9,10] or (in more modern language) as unconventional. This last word sometimes is used in relation to superconductors in which pairing mechanisms other than electron–phonon is the operative [11]. Slightly more formally, the unconventional character of the superconductivity means that not only the gauge $U(1)$ symmetry is spontaneously broken below the transition temperature as in all superconductors but also other symmetries are broken. Among them the TRS plays a special role.

Experimentally unconventional superconductors are characterized by the non-exponential temperature dependence of the thermodynamic characteristics, as e.g., the penetration depth $\lambda(T)$, absence of the Hebel–Slichter peak in the relaxation rate, etc. Most notably the existence of superconductivity can be tuned by external parameters like the pressure or doping. Additionally,

phase diagrams of many different families of unconventional superconductors on the temperature (T) control parameter (x) plane show profound similarities. This is visible in Figure 1, where we have sketched the phase diagrams of heavy fermions, high-temperature, and organic superconductors. Moreover, the phase diagram of iron-based superconductors is also of a similar character with doping serving as the control parameter.

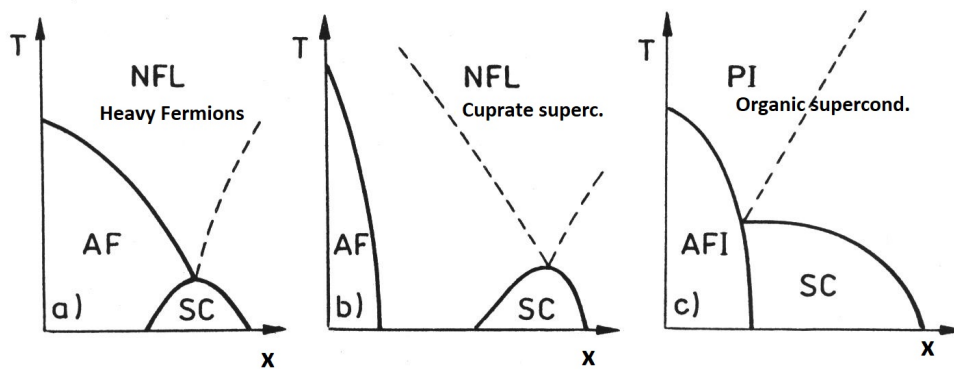


Figure 1. The phase diagrams of three families of superconductors: heavy fermions, high-temperature cuprates, and organics. The control parameter x denotes pressure p in panel (a,c) and the doping in case of cuprate superconductors (b). It has to be added that the phase diagram of iron-based materials is of similar shape with x denoting the doping. Various phases are known as NFL—non-Fermi liquid, AF(I)—anti-ferromagnetic (insulator), PI—paramagnetic insulator, and SC—superconductor.

Recently, the increased interest is observed in the detection and understanding of the TRS breaking and its relation to other symmetries. In the last few years, a number of TRS breaking superconductors with chiral [12] and other order parameters breaking the TRS have been identified. One of the best-known examples of TRS breaking superconductors is Sr_2RuO_4 . This material is believed to have the spin-triplet odd parity superconducting order parameter with \mathbf{d} vector along the c -crystallographic axis $\mathbf{d}(\mathbf{k}) \sim (k_x \pm ik_y)\hat{e}_z$. This order parameter is called chiral because its phase winds in a clockwise or counter-clockwise sense by $\pm 2\pi$ as \mathbf{k} -vector moves about the k_z axis on the Fermi surface. It breaks TRS. This is so, as the inversion of time $t \rightarrow -t$ and the complex conjugation change the order parameter due to the complex i factor; the ground state is thus doubly degenerate.

The scientific importance of the chiral superconductors is in part related to the fact that they have been proposed [12] to host Majorana particles and other quantum states of interest [13]. Majorana particles are real solutions of the Dirac equation. Predicted by the Ettore Majorana, they have never been observed in vacuum [14], but have been proposed to exist in chiral superconductors as a zero energy modes. This makes chiral superconductors important examples of topologically non-trivial systems. Due to their non-abelian statistics, Majorana fermions may find applications in the context of quantum computing [15]. It is mainly Sr_2RuO_4 which is considered an important example of the system with chiral order parameters which break TRS. The material is also expected to carry signatures of non-trivial topology. Discussing this system we concentrate mainly on the Kerr effect paying special attention to its multi-orbital character. This is because the recent discovery of the novel [16,17] intrinsic mechanism of the Kerr effect operating in strontium ruthenate and possibly other systems.

The paper is organized as follows. In Section 2, we review the early and recent experimental discoveries of superconductors which break TRS. Our studies of various aspects of superconductivity in Sr_2RuO_4 are reviewed in Section 3. Here we also discuss the appearance (in many systems) of zero energy states of origin possibly not related to the Majorana physics (see Section 3.4). The multi-orbital/multi-band mechanism of the Kerr effect is introduced in Section 4 with application to strontium ruthenate. We end up with a few general observations and the summary of the paper in Section 5.

2. TRS Breaking in Superconductors

The detection of the TRS breaking necessarily means the unconventional nature of superconductivity. This is so, because in those superconductors the spontaneous breaking of U(1) gauge symmetry is often accompanied by breaking additional symmetries: time reversal or spatial. For example, the d-wave character of the order parameter in high-temperature superconductors (HTS), as confirmed again recently with a new dielectric resonator method [18], provides a case of spatial symmetry breaking. The crystals of HTS have a four-fold symmetry axis perpendicular to their *ab* plane but the d-wave order parameter $\Delta(\mathbf{k}) = \Delta_0(T)[\cos(k_x a) - \cos(k_y a)]$ features only the two-fold one.

2.1. Methods for Detecting TRS Breaking

There are a few established methods to detect the existence of TRS breaking in superconductors. These are muon spin rotation and relaxation (μ SR), polarised neutron scattering, detection of circular currents, and the polar Kerr effect [19]. Recently, there appeared different additional proposals to detect the TRSB state experimentally. One of them is by laser pulse probe [20], when one expects changes of the condensate properties around the laser heated spot. The modifications depend on the symmetry of the order parameter. Depending if it is of s-wave or p-wave, one expects different patterns of the magnetic field, which can be measured. Another proposal relies on the detection of the diamagnetic response of multi-band superconductors [21]. According to the authors, the current induced magnetic flux response could in principle be used to detect TRS breaking in the ground state.

The method most often applied to detect TRS breaking at the onset of the superconducting state is the muon spin rotation and relaxation (μ SR). If the surface of the superconductor can be suitably prepared the polar Kerr effect can also be measured. One or both of these techniques have been applied to different superconducting systems and resulted in observations indicating TRS breaking in Sr_2RuO_4 , UPt_3 , URu_2Si_2 and many more superconductors as indicated in Table 1. Recently the epitaxial bilayers of Bi and Ni [22,23] were found not only to show superconductivity, but also TRS breaking superconducting order parameter. Neither the mechanism nor the superconducting state in the system is uniquely identified. We mention the observations indicating TRS breaking near the pseudogap phase of HTS [24], which might be caused by the magnetic order in crystals [25,26] or recently discovered [27] slowly fluctuating magnetic fields of intra-unit-cell origin in the same region of the phase diagram.

Superconductors which break TRS may also have distinctive responses to other disturbances like local temperature bias $\Delta T(r)$, etc. It has been found [28] that the thermoelectric response of TRS breaking superconductors to $\Delta T(r)$ depends on the thermally induced magnetic field with a profile that is sensitive to the presence of domain walls and anisotropy of superconducting states. If the heating process is non-stationary, the time dependent B field produces an electric field. As a result there appears to be a charge imbalance in the different bands. In view of the puzzles related to understanding thermopower in superconductors [29–32] and hybrid structures [33,34], this is an interesting result worthy of deeper analysis.

The μ SR technique is a local, very sensitive probe [35,36] detecting tiny magnetic fields in the bulk of solid samples. Most experiments use positively charged muons with the energy of a few MeV. The beam is spin polarised. Being a local probe, μ SR is very sensitive to inhomogeneities of the magnetic properties and is able to detect various phases in the sample. They are reflected by the appearance of the different components in the μ SR signal. The muons implanted into the sample undergo fast deceleration. After the time comparable to their lifetime ($\approx 2.2 \mu\text{s}$), the muons in the sample decay via parity non-conserving weak interaction process into positron and two neutrinos. The emission probability of the positron depends on the angle between the μ^+ spin and the positron trajectory. The asymmetry of the probability distribution depends on the muon beam polarisation P_{μ^+} . The latter becomes time dependent if the implanted μ^+ is at the stopping site subject to local

magnetic field rotating its spin. The measured signal is thus a function of the time dependent spin correlation function

$$G(t) = \frac{\langle \vec{S}(t)\vec{S}(0) \rangle}{S^2(0)}, \quad (1)$$

which depends on the magnitude of the internal **B** field, its distribution and time evolution. The time dependent counting rate can be written as

$$N_{e^+}(t) = B + N_0 \left[1 + aG(t)\cos(\omega_\mu t + \phi) \right], \quad (2)$$

with B denoting the background, ϕ the geometry dependent phase shift, ω_μ the Larmor frequency, a the asymmetry parameter and N_0 the normalization constant. Muons stopped at different sites precess with different Larmor frequencies.

For immobile muons, the line-shape is Gaussian, while the motional narrowing is observed for mobile muons when the field fluctuations are averaged out leading to the exponential decay of polarisation. The long range magnetic order in the sample shows up as a precession signal in the μ SR data. The time dependence found in the experimental data on LaNiC₂ sample [37] lacks such term and has been described by the function

$$N_{e^+}(t) = B + A_0 G_{KT} e^{-\lambda t}, \quad (3)$$

where A_0 denotes the initial asymmetry and $G_{KT}(t)$ is the Kubo–Toyobe function describing the effect of local fields resulting from randomly oriented nuclear moments. The parameter λ in this experiment depends on temperature and arises from electronic moments in the system. In the superconductors breaking TRS, the parameter λ starts to depend on temperature below superconducting transition temperature. Its T dependence provides valuable information on the symmetry of the order parameter. The more detailed discussion of the μ SR technique and its application to study unconventional superconductors can be found in the recent review [38].

The magnetic polar Kerr effect (PKE) measures the rotation of linearly polarized light reflected from a magnetized material at normal incidence. If the non-zero signal is measured in zero external magnetic field, one talks about spontaneous dichroism. The dichroism is the property of the material that the absorption of light depends on the polarisation. This is due to the fact that complex indices of refraction for left and right circular polarisations, which make up the linear one, are different. The PKE is known to occur in systems which break TRS like ferromagnets but also in materials which break inversion symmetry (as e.g., sugar). To quantify the effect, one calculates the power absorbed by the system for a given polarisation of the light beam perpendicular to the sample surface. Making use of the time dependent perturbation theory and dipole approximation, one finds [39,40] that the difference of the power absorbed for two polarisations of light at frequency ω is proportional to the imaginary part of the Hall conductivity $\sigma_{xy}(\omega)$, while the sum of the two contributions gives the real part of it. This agrees with the general result that in the linear regime the absorption of light is generally described by the conductivity tensor $\hat{\sigma}(\omega)$.

Another way to see how the PKE is related to the frequency dependent Hall transport coefficient $\sigma_{xy}(\omega)$ is to note that the reflection coefficient $|r|$

$$|r| = \frac{|n - 1|}{|n + 1|}, \quad (4)$$

is directly related to the polar Kerr angle θ_K [41]

$$\theta_K = \frac{4\pi}{\omega} \text{Im} \frac{\sigma_{xy}(\omega)}{n(n^2 - 1)}, \quad (5)$$

where n is the complex refraction coefficient. On the other hand, the polar Kerr angle (5) can be shown [42] to read

$$\theta_K = \frac{4\pi\omega^2 \text{Im}\sigma_{xy}(\omega)}{\sqrt{\epsilon_\infty\omega^2 - \omega_{ab}^2} [(\epsilon_\infty - 1)\omega^2 - \omega_{ab}^2]}, \quad (6)$$

for light frequency higher than the in-plane plasma frequency ω_{ab} , and

$$\theta_K = -\frac{4\pi\omega^2 \text{Re}\sigma_{xy}(\omega)}{\sqrt{\omega_{ab}^2 - \epsilon_\infty\omega^2} [(\epsilon_\infty - 1)\omega^2 - \omega_{ab}^2]}, \quad (7)$$

in the low frequency regime ($\omega < \omega_{ab}$). The experimental details related to the measurements of the PKE in TRS breaking superconductors, together with the relevant examples of the temperature dependence of θ_K , have been presented by Kapitulnik et al. [19,43].

The proper analysis of the Kerr effect requires careful consideration of the symmetries. Due to the delicate relation between reciprocity and TRS, a number of proposals turned out to be not as valid as discussed here [44]. For example, the gyrotropy, being a result of natural optical activity of the materials can not lead to the non-zero Kerr response. Natural optical dichroism, as in sugar, is expressed by the Kubo linear response formula for finite wave vectors \mathbf{q} of light and its observation require zero magnetic field. The wave vector \mathbf{q} , frequency ω and magnetic field \mathbf{B} dependent conductivity tensor is subject to the general Onsager symmetry relations

$$\sigma_{i,j}(\mathbf{q}, \omega, \mathbf{B}) = \sigma_{j,i}(-\mathbf{q}, \omega, -\mathbf{B}). \quad (8)$$

Without external or internal magnetic fields, $\mathbf{B}=0$, this leads [45] to the relation $\sigma_{i,j}(\mathbf{q}, \omega, \mathbf{B} = \mathbf{0}) = \sigma_n \epsilon^{ijl} q_l$ (here ϵ^{ijl} denotes the totally anti-symmetric tensor and the summation over repeated indices is implicit) and is an example of the natural dichroism. Natural dichroism depends on the direction of light and the chirality of the underlying molecules. On the other hand, the Kerr rotation (the same is true for the Faraday effect) is measured for $\mathbf{q} = 0$. It relies upon the TRS breaking resulting from magnetic field or magnetisation. The Onsager symmetry provides the relation $\sigma_{i,j}(\mathbf{q} = 0, \omega, \mathbf{B}) = \sigma_K \epsilon^{ijl} B_l$. In superconductors the same relation is valid with the spontaneous magnetisation [46] replacing the \mathbf{B} field. σ_n and σ_K above denote scalars characterising natural (n) and Kerr (K) response of the system. These may depend on temperature for example.

2.2. Superconductors with TRS Broken State

Table 1 gives a summary of TRS breaking materials together with some of their properties. In the table, we indicate the method(s) used to detect TRS, the superconducting transition temperature and an important crystallographic aspect, namely the existence or not of the center of inversion. The systems with the center of inversion are known as centrosymmetric (C) and those without it as non-centrosymmetric (NC). We use the word centrosymmetric to denote the system with such crystallographic point group, that for every point in the unit cell there exists another indistinguishable point e.g., a point (x, y, z) is indistinguishable from the point $(-x, -y, -z)$. The point in the unit cell having this property is called a center of inversion and the corresponding point group is said to have inversion symmetry. The crystals lacking the center of inversion are called non-centrosymmetric.

The information on the superconducting order parameter in superconductors listed in Table 1 is mostly scarce. They are subject to ongoing intensive research. Some of the compounds mentioned in Table 1 have been known for many years, while others have been discovered only recently. Here we add a few remarks concerning the properties of some materials and their families. For more comprehensive discussion, we direct the reader to the original cited literature.

The superconductivity in URu₂Si₂ has been discovered [47] in 1986, but most of the work has been devoted to the 17.5 K anomaly observed in this material and termed “hidden” order. The identification of it is the subject of on-going vigorous work and debate [48]. One of the first examples where the

broken TRS has been detected [49–51] is UPt_3 . This superconductor has a rich phase diagram on the temperature–magnetic field plane with three different phases (named A, B and C) characterised by the unique nodal structures of the superconducting order parameter [52]. It is well established that the TRS is broken in one of these phases.

The effect of disorder on the TRS broken state is not known in detail yet. Typically the disorder seems to decrease the internal fields. In the two alloy series, $\text{Pr}_{1-y}\text{La}_y\text{Os}_4\text{Sb}_{12}$ and $\text{Pr}(\text{Os}_{1-x}\text{Ru}_x)_4\text{Sb}_{12}$, the magnetic field appearing below T_c and revealed by μSR measurements has been found to initially decrease linearly with solute concentration [53]. It has been also established that Ru doping is considerably more efficient in the decreasing magnetic field than La doping, with a 50% faster initial decrease. The data suggest that broken TRS state is suppressed for Ru concentration $x \geq 0.6$ but persists for essentially all La concentrations. The detailed changes of the superconducting properties of the alloys are needed to understand this behavior.

Table 1. Time reversal symmetry (TRS) breaking superconductors and their properties. We indicate the method of detection of TRS breaking, the structure of the material if it is centrosymmetric (C) or non-centrosymmetric (NC), the T_c . The last entry provides the remarks concerning the structure of the order parameter.

Material	Detection	Structure	T_c [K]	sc State
Sr_2RuO_4	μSR [54], Kerr [55]	C	1.5	nodal, spin triplet, $p_x \pm ip_y$ [6]
UPt_3	μSR [49], Kerr [56]	C	0.54	spin triplet
URu_2Si_2	Kerr [57]	C	1.5	[47]
$\text{PrOs}_4\text{Sb}_{12}$	μSR [58], Kerr [59]	C	1.8	[60]
$\text{PrPt}_4\text{Ge}_{12}$	μSR [61]	C	7.9	
$\text{Pr}_{1-y}\text{La}_y\text{Os}_4\text{Sb}_{12}$	μSR [53]	C	~ 1	
$\text{Pr}(\text{Os}_{1-x}\text{Ru}_x)_4\text{Sb}_{12}$	μSR [53]	C		
$\text{Ba}_{0.27}\text{K}_{0.73}\text{Fe}_2\text{As}_2$	μSR [62]	C	13	$s + is$ or $s + id$ (?)
LaNiGa_2	μSR [63]	C	2.1	
Re	μSR [64]	C	2.7	fully gapped
$\text{Re}_{0.82}\text{Nb}_{0.12}$	μSR [64]	C	8.8	
SrPtAs	μSR [65]	NC (locally)	2.4	$d + id$
LaNiC_2	μSR [37,66]	NC	2.7	multi-gapped, non-unitary triplet
$\text{Lu}_5\text{Rh}_6\text{Sn}_{18}$	μSR [67]	C	4.0	$d + id$ (?)
La_7Ir_3	μSR [68]	NC	2.25	
La_7Rh_3	μSR [69]	NC	2.65	
Re_6Zr	μSR [70,71]	NC	6.75	
Re_6Hf	μSR [72]	NC	5.91	s-wave
Re_6Ti	μSR [73]	NC	6.0	
$\text{Re}_{24}\text{Ti}_5$	μSR [64]	NC	6	s-wave
Zr_3Ir	μSR [74]	NC	2.2	single gap, nodeless
$\text{Pr}_{1-x}\text{Ce}_x\text{Pt}_4\text{Ge}_{12}$	μSR [75]	NC?		
Bi/Ni (bilayers)	Kerr [22]	NC	3.6	$d_{xy} \pm id_{x^2-y^2}$ (?)

It is visible from Table 1 that many superconductors with Re as one of the components belong to NC compounds and at the same time break TRS. This raises the question about the possible relation between both symmetries and the reasons, while so many Re TM (TM –transition metal) alloys feature such behavior. To elucidate the issue, the authors [64] have performed the comparative studies of elemental Re superconductor ($T_c = 2.7$ K) with the center of inversion and the $\text{Re}_{0.82}\text{Nb}_{0.12}$ alloy ($T_c = 8.8$ K) without it. Both superconductors have been studied with the μSR technique and small but well defined magnetic fields were detected below T_c indicating the spontaneous TRS breaking in both superconductors. The authors of the paper write that the lack of the inversion symmetry is not essential for the appearance of TRS breaking. Such conclusions also seem to follow from the data presented in the table, where equally many of the TRS breaking materials belong to both classes of crystals. On the other hand, the lack of TRS strongly constrains the allowed symmetry of the superconducting order parameter. This together with the temperature dependence of the specific

heat and other thermodynamic and transport characteristics allows us to judge the presence of the gaps in the order parameter. The details of the symmetry of the order parameter in elemental Re superconductor and its superconducting compounds are still unknown. However, the lack of TRS in Re compounds seem to be crucially related to the presence of this element. To further explore the role of Re in the Re TM compounds, the binary Re $_{1-x}$ Mo $_x$ alloy series have been prepared and shown [76] to be superconducting for all concentrations x of Mo with the highest $T_c = 12.4$ K for $x \approx 0.6$. Depending on x different crystallographic structures have been found. Among them the non-centrosymmetric α -Mn has been obtained. Superconductivity in non-centrosymmetric materials has been reviewed recently [77].

3. Sr $_2$ RuO $_4$: Puzzles, Solutions, and Still Open Issues

The superconductivity in strontium ruthenate was discovered 25 years ago and understanding it is still challenging. The title of the recent review “*Even odder after twenty-three years: the superconducting order parameter puzzle of Sr $_2$ RuO $_4$* ” summarizes well [78] the state of the art in our understanding of its superconducting properties. The normal state seem to be of the Fermi liquid variety and well behaved, although the issues related to the strength of electron correlations and spin-orbit coupling are not quite clear [79–82]. Beside the above mentioned paper, many other excellent reviews on nearly all aspects related to strontium ruthenate exist [12,83–86]. Thus we shall concentrate on a few less common issues, namely the observation and understanding of the Kerr effect in the material.

After the discovery of the superconductivity in Sr $_2$ RuO $_4$, the hope was that its understanding would shed light on the high-temperature cuprate superconductors. Both share the same crystallographic perovskite structure. This was supported by the observation that at low temperature strontium ruthenate is a metal and behaves as an anisotropic and possibly correlated but otherwise well defined Fermi liquid [87]. Later on it turned out that Sr $_2$ RuO $_4$ is much more complicated with three bands being in play, possibly hosting spin triplet p-wave superconductivity. The first hint on the unconventional character of superconductivity has been provided by the extreme sensitivity of T_c on non-magnetic disorder [88].

The Fermi surface of the materials consists of three sheets known as α , β , and γ . The first two are of one dimensional origin and result from hybridised d_{xz} and d_{yz} Ru orbitals, while the last one from d_{xy} orbitals. This variety of orbitals has resulted in a discussion about the active bands and the role various orbitals play in the superconducting state [89–91]. To understand experimental results showing the existence of line nodes, or at least deep minima in the quasi-particle density of states, it has been proposed [90] that a full gap exists in the active band, which is that derived from d_{xy} orbitals and the line nodes develop in passive bands by the inter-band proximity effect. The multi-band aspects of superconductivity in this system, however, are of different variety from that considered in heavy fermion materials [92–94], albeit some similarities can be found. In particular all three bands are partially filled and the electron–electron interactions are of comparable magnitude in all of them, while in heavy fermion materials, the conduction band is not correlated while the narrow, non-dispersing band is strongly correlated. The discussion about the role of active vs. passive bands continues [95–97]. It is not unrelated to the studies of spin fluctuations in the material and the relative role of Coulomb interactions in different orbitals, mentioned earlier.

Kallin and Berlinsky, finishing their review on chiral superconductors [12], wrote “*one would also like to have detailed information of where the low-lying excitations in Sr $_2$ RuO $_4$ are in momentum space...*”. The recent experiments [98] might provide, at least, a partial answer to that issue. Thus, even though the origin of the spin triplet pairing in strontium ruthenate is still under debate, the discovery of the low energy modes [98] seem to give a novel argument in favor of the earlier proposals [99,100] pointing out that the ferromagnetic spin fluctuations operating in the material are responsible for its superconducting instability. Spin fluctuations have been studied in numerous papers [101–104] without clear cut conclusions. The relative importance of the ferro- vs. anti-ferromagnetic fluctuation has also been probed [105]. The conclusion of the recent paper [106] studying this issue by means

of polarized inelastic neutron scattering is that “spin fluctuations alone are not enough to generate a triplet state”. This is in opposition to the results presented by Akebi et al. [98] and calls for further detailed analysis.

3.1. Modelling of Strontium Ruthenate

In view of the controversies about the microscopic mechanism of superconductivity in strontium ruthenate, we have modeled the system by using precise knowledge related to its spectrum and assumed the phenomenological interaction parameters leading to the p-wave superconducting state in all three bands. The details have been described in the number of papers [46,107–111] and I shall not repeat them here. The Hamiltonian of the system written in the orbital basis reads

$$\begin{aligned} \hat{H} = & \sum_{ijmm',\sigma} ((\varepsilon_m - \mu)\delta_{ij}\delta_{mm'} - t_{mm'}(ij)) \hat{c}_{im\sigma}^+ \hat{c}_{jm'\sigma} \\ & + i\frac{\lambda}{2} \sum_{i,\sigma\sigma'} \sum_{mm'} \varepsilon^{xmm'} \sigma_{\sigma\sigma'}^x c_{im\sigma}^+ c_{im'\sigma'} \\ & - \frac{1}{2} \sum_{ijmm'} U_{mm'}^{\alpha\beta,\gamma\delta}(ij) \hat{c}_{im\alpha}^+ \hat{c}_{jm'\beta}^+ \hat{c}_{jm'\gamma} \hat{c}_{im\delta}, \end{aligned} \quad (9)$$

where m and m' refer to the three Ru t_{2g} orbitals $a = d_{xz}$, $b = d_{yz}$ and $c = d_{xy}$; i and j label the sites of a body centered tetragonal lattice. The hopping integrals $t_{mm'}(ij)$ and site energies ε_m were fitted to reproduce the experimentally determined Fermi surface [112,113]. λ is the effective Ru 4d spin-orbit coupling parameter, and the effective Hubbard parameters $U_{mm'}^{\alpha\beta,\gamma\delta}(ij)$ are generally spin as well as orbital dependent. In its simplest version, the model uses just two effective Hubbard interaction parameters, both of which are completely determined by the requirement to fit the experimental T_c . One of the parameters is responsible for the effective attraction of electrons occupying d_{xy} orbitals of in plane Ru atoms, while the other is for the attraction between electrons residing in out of plane Ru orbitals.

One of the puzzling behaviors of strontium ruthenate has been found in measurements of the electronic spin susceptibility in external magnetic field parallel and perpendicular to the ab plane of the material. The spin susceptibility of the spin-triplet superconductors is known to have matrix (3×3) structure with entries depending on the direction of the \mathbf{d} -vector. For standard spin-triplet odd parity chiral state the \mathbf{d} -vector is of the form [114,115]

$$\mathbf{d}(\mathbf{k}) = (\sin k_x \pm i \sin k_y) \hat{\mathbf{e}}_z, \quad (10)$$

and is directed along crystallographic c -axis, while for the helical states of the variety,

$$\begin{aligned} \mathbf{d}(\mathbf{k}) &= (\sin k_x, \sin k_y, 0) \\ \mathbf{d}(\mathbf{k}) &= (\sin k_y, -\sin k_x, 0) \end{aligned} \quad (11)$$

it is lying in the (a,b) -plane of the strontium ruthenate. The early ^{17}O Knight shift experiments performed in (ab) plane magnetic fields [116] and neutron scattering experiments [117] both observed a constant susceptibility below T_c consistent with chiral triplet pairing state with \mathbf{d} along c -axis. On the other hand, the measurements by Murakawa et al. [118] in magnetic field parallel to the c -axis also observed spin susceptibility below T_c of the same value as in the normal state. This immediately indicates that either the superconducting state is not chiral, or \mathbf{B} field induces the phase transition from the chiral to the helical state. Using the three band model with relatively small but realistic spin-orbit coupling, we have argued [119,120] that the \mathbf{d} -vector rotates and the phase transition is expected. The calculated entropy jump at low temperatures has been found to be very small, so the transition could be undetected in specific heat experiments.

3.2. Horizontal or Vertical Line Nodes?

Small angle neutron scattering studies [121] provide support to the anisotropic multi-band superconducting state with gap nodes or at least deep minima. The authors inferred the multi-band

behavior from the superconducting anisotropy in Sr₂RuO₄. The anisotropy is hardly temperature dependent but increases for higher fields (≥ 1 T). This paper found evidence from vortex lattice distortion that the intrinsic superconducting anisotropy between the c axis and the Ru–O basal plane being of the order 60 is in agreement with that measured [122] by the ratio of coherence length $\xi_{ab}/\xi_c \approx 60$, but exceeds the magnetic field anisotropy $H_{c2}^{ab}/H_{c2}^c \approx 20$. In line with the above findings is the work of Kallin et al. who have shown [123] that if there are no horizontal nodes in the superconducting order parameter of Sr₂RuO₄, it is particularly difficult to reconcile chiral-p-wave order with residual thermal conductivity data. The model (9) leads to the horizontal nodes in the superconducting order parameter. The order parameter has a number of intra- and interorbital components. They are written as

$$\Delta_{cc}(\mathbf{k}) = \Delta_{cc}^x(T) \sin k_x \pm i\Delta_{cc}^y(T) \sin k_y \quad (12)$$

for $c(=d_{xy})$ orbitals and,

$$\Delta_{mm'}(\mathbf{k}) = (\Delta_{mm'}^x \sin \frac{k_x}{2} \cos \frac{k_y}{2} \pm i\Delta_{mm'}^y \sin \frac{k_y}{2} \cos \frac{k_x}{2}) \cos \frac{k_z c}{2} \quad (13)$$

for $m, m' = a, b$ or d_{xz} and d_{yz} orbitals forming α and β Fermi sheets. The experiments [124] showing the existence of vertical line nodes in Sr₂RuO₄ provide a good reason for further analysis of the gap nodes as it is not clear if the vertical anisotropy of the gaps as given by (13), together with the warping of the essentially cylindrical Fermi surface is enough to understand the measurements. For recent group–theoretical analysis of the gap nodes in tetragonal crystal see [125].

3.3. Surface Magnetic Fields

As already indicated, the μ SR and the polar Kerr effect experiments point towards the appearance of spontaneous magnetic fields inside the chiral strontium ruthenate superconductor. According to the expectations for such superconductors at their surfaces, at domain walls, and near impurities [126], one should observe a small magnetic field. Despite many experimental efforts none of the measurements has found such surface magnetic fields [127–129]. For example in the paper [127], the authors used sensitive scanning Hall bar and superconducting quantum interference device microscopies and did not detect any expected supercurrents. Negative results have been obtained in similar measurements for Sr₂RuO₄ and PrOs₄Sb₁₂ [128,130] and suggested that the size of the chiral domains might be much smaller than expected. The paper [129] imposes an upper limit of ± 2.5 mG on the magnitude of spontaneous magnetic fields at the well-defined edges of a mesoscopic disk. It is important to note that despite the lack of surface fields, the superconductivity-related TRS breaking fields in the bulk have been unequivocally observed by muon spin rotation and the Kerr effect (see Table 1). Judging from the value of the Kerr angle, the fields appear to be really small.

On the theory side there appeared a number of papers trying to find reasons for such behavior [131–133]. Recent studies [134] have shown that the surface flux pattern in chiral superconductors is not a universal feature, but instead it depends on many parameters describing the system. As a consequence the magnitude of the expected magnetic fields may differ from case to case and be smaller than expected earlier [135].

3.4. Topology Related Aspects—A Few Remarks

Strontium ruthenate has been considered as one of the systems with non-trivial topological properties [126] in the form of half-vortices eventually hosting Majorana particles [136] with interesting topological signatures [13]. The Majorana modes are detected experimentally as zero energy/bias features in scanning tunnelling spectroscopy measurements (STS). In view of the recent intensive work aimed at the identification, properties, and possible applications of topological materials, it is worth mentioning that many real and artificially engineered systems, whether superconducting or not,

seem to show signatures of Majorana particles [137] or at least zero bias conductance peaks [138] of various origin [139]. The earlier mentioned [95–97] ambiguity on passive and active bands in Sr_2RuO_4 is important as it affects the existence or not of the topological half-vortices with their zero-energy states hosting Majorana particles. If the superconducting state arises from the one-dimensional like bands [95] formed by d_{xz} and d_{yz} orbitals than the chiral state is expected to be topologically trivial without Majorana edge states. On the other hand, the d_{xy} related superconducting state is expected to be topologically non-trivial.

The artificial superconducting structures may also break TRS. The TRS breaking seem to be of intrinsic character in superconducting bilayers [22]. It results from the presence of magnetic subsystem in hybrid magnet-superconductor interfaces [137]. The zero energy modes and the superconducting-like energy gap found experimentally in the studies of $\text{Pb}_{1-x-y}\text{Sn}_y\text{Mn}_x\text{Te}$ [138] appear at the topological surfaces of diamagnetic, paramagnetic, and also ferromagnetic samples.

However, clear identification of zero-bias peak from spectroscopic measurements as a Majorana bound state is demanding if not impossible. This is because there exist a number of effects, such as the Kondo effect, producing virtually the same STS/STM spectra. This brings about the ongoing debate on the origin of the zero-bias conductance peak revealed in a series of point contact experiments at the surface of topological semiconductors and semi-metals [138,140,141]. Although most of the authors implied that Majorana excitations could be seen, there was other non superconductivity, despite topology-related explanations of such spectra [139]. The detailed calculations showing the emergence of zero-energy states in the trivial phase of a short nano-wire junction with strong spin-orbit coupling and magnetic fields have been presented recently [142]. The forming of zero energy state in the model of this paper requires strong coupling between the nano-wire and two superconductors.

4. Understanding the Kerr Effect in Sr_2RuO_4 —Multi-Orbital Mechanism

Shortly after the measurements of the Kerr signal in Sr_2RuO_4 a number of theoretical papers appeared trying to understand its origin, magnitude, and temperature dependence. For references and a critical discussion see [42,143]. As noted earlier, the existence of the Kerr signal is intimately related to the anomalous frequency dependent Hall effect $\sigma_H(\omega)$. Due to the TRS breaking state in superconductors one expects appearance of spontaneous magnetic fields and thus the Hall effect. The latter transport coefficient, however, requires that the charge in an electric field directed along, say x direction, to move also in y direction as in the standard Hall effect in a \mathbf{B} field. In the presence of the magnetic field, the perpendicular (i.e., in the y direction) motion is related to the Lorentz force. However, in the present case, the chiral state responsible for TRS breaking state is a result of internal interactions between the electrons. Thus the required force has to result from effective internal interactions inducing the chiral $k_x \pm ik_y$ state. This, however is impossible in the Galilean invariant system. This argument about the absence of such skew scattering in one-band Galilean invariant system has been put forward by Read and Green [136]. Good discussion of different constraints related to the observation of the Kerr effect can be found in [44]. Later on, we shall present more formal argument showing vanishing of the Hall conductivity in one band chiral superconductor.

It is important to remember that the breaking of TRS is a necessary but not sufficient condition for the observation of the Kerr effect. This is also true for magnetic systems, where spin-orbit interaction is a required additional ingredient [144] for the Hall effect to exist. It turns out that the similar situation is observed in the TRS breaking superconductors. To observe the Kerr effect, additional factors have to contribute. In the literature, there were various mechanisms discussed. These included particle–hole asymmetry [145], the order parameter collective mode response [146], the impurity scattering leading to non-trivial vertex corrections and multi-orbital effects and the final size of the laser spot.

The ac Hall effect in chiral superconductors requires the breaking of the translational invariance and this is achieved by impurities as proposed originally by Goryo [147] and later elaborated by Lutchyn et al. [42,143]. Other possibility is provided by the many orbital or many band models.

Earlier not considered mechanisms of the Kerr effect have been independently proposed by two groups [16,17].

The simple, formal argument on the absence of ac Hall conductivity $\sigma_H(\omega)$ has been given by Taylor and Kallin [16]. These authors have noted that $\sigma_H(\omega)$ is given by the antisymmetric part of the current–current correlation function $\pi_{xy}(\mathbf{q}, \omega)$

$$\sigma_H(\omega) = \frac{i}{2\omega} \lim_{q \rightarrow 0} [\pi_{xy}(\mathbf{q}, \omega) - \pi_{yx}(\mathbf{q}, \omega)]. \quad (14)$$

The correlator itself can be written in terms of the velocity matrices \hat{v}_x and \hat{v}_y and matrices of the Green functions \hat{G} of the superconducting system as

$$\pi_{xy}(\mathbf{q}, i\omega_n) = e^2 T \sum_{\mathbf{k}, i\omega_l} \text{tr} [\hat{v}_x \hat{G}(\mathbf{k}, i\omega_l) \hat{v}_y \hat{G}(\mathbf{k} + \mathbf{q}, i\omega_l + i\omega_n)]. \quad (15)$$

It follows that σ_H vanishes for diagonal velocity matrices \hat{v}_x and \hat{v}_y as they commute with the Green function matrices. The critical overview of various attempts to calculate the Kerr effect can be found in [148].

Two different approaches have been used and two different models sharing, however, the multi-band/multi-orbital character have been studied by the two groups [16,17] proposing the novel mechanism of the Kerr effect. The results [149–151] provide a novel description of the anomalous ac Hall conductivity and are valid for virtually all superconductors. The prerequisite is the TRS breaking order parameter and a multi-band one with non-zero inter-orbital/inter-band velocity matrices.

While the Kubo approach has been used in [16], we [17] have calculated the Kerr effect from the definition of the optical dichroism [39,40]. In this formalism, the conductivity tensor can be expressed in terms of the difference of the electromagnetic power absorption $P(\omega, \vec{\epsilon})$ for light of left and right circular polarizations, $\vec{\epsilon}_L$ and $\vec{\epsilon}_R$, respectively,

$$\text{Im}[\sigma_{xy}(\omega)] = \frac{1}{VE_0^2} [P(\omega, \vec{\epsilon}_L) - P(\omega, \vec{\epsilon}_R)]. \quad (16)$$

The power has been calculated from the Fermi golden rule with the dipole matrix elements evaluated between the Bogolubov-de Gennes states.

The quantitative analysis of the effect with realistic parameters of Sr_2RuO_4 lead to the Kerr angle of order of 60 nrad in agreement with experimental data finding $\theta_K \approx 60\text{--}90$ nrad. We have also calculated the temperature dependence of the signal and found that $\theta_K \propto \Delta^2(T) \approx 1 - \frac{T}{T_c}$ for temperature close to the the superconducting transition temperature. The existence of the Hebel–Slichter like peak in the temperature dependence of θ_K predicted in the paper [17] has not been confirmed, and much less pronounced anomalies have been found for light frequencies very close to the threshold frequency [151]. Interestingly, the threshold frequency in the model is not related to the value of the superconducting gap, but is of the order of the smallest value of the hybridisation parameters between the orbitals. It is important to mention that the symmetry analysis of the problem clearly shows [151] that $\Delta_{bb}^y = i\Delta_{aa}^x$ and $\Delta_{aa}^y = i\Delta_{bb}^x$, while there is no specific relation between $\Delta_{aa/bb}^x$ and $\Delta_{aa/bb}^y$.

The inter-orbital mechanism seems to be especially well suited for the understanding of the Kerr effect in strontium ruthenate, which is perhaps the cleanest superconductor ever studied and the concurrent mechanism relying on higher order impurity scattering is not efficient. The novel mechanism of the polar Kerr effect discovered during studies of the Kerr effect in this superconductor is of general importance and its validity for the semi-quantitative description of the effect in UBe_3 has been recently demonstrated [152].

5. Summary

We have reviewed aspects related to TRS breaking in superconductors including Sr_2RuO_4 , UPt_3 , and other newly discovered systems. One has to note that the family of materials with this property is growing very fast. Moreover, many compounds belong to the non-centro-symmetric crystals. This calls for better understanding of the interplay between various symmetries in superconductors.

We have briefly described standard techniques used to identify TRS breaking in superconductors, namely the μSR and the Kerr effect. We have discussed some of the many puzzling characteristics of strontium ruthenate (Sr_2RuO_4), one of the cleanest and best studied superconductors with TRS breaking state below T_c . The special attention has been paid to the discovery of the novel mechanism of the Kerr effect [16,17] and its application to Sr_2RuO_4 . However, many of the recent discoveries [153–164] have been left, partly due to lack of space in this short review. We only mention that the recent work [163] has established close relations between the Kerr rotation and odd-frequency superconductivity. Both are emerging from the same finite hybridization between different orbitals. Thus Sr_2RuO_4 appears as one of the first bulk materials hosting odd-frequency superconductivity.

The discussed multi-orbital mechanism of the Kerr effect is universally valid in both clean and dirty materials. In view of the recent interests in the study of TRS breaking in superconductors, it would be of great interest to evaluate the relative share of the impurity and inter-orbital contributions to the measured signal. This should be possible by means of the controlled disordering and the concomitant measurements of the Kerr angle of one of the many novel superconductors with the TRS breaking order parameter.

Funding: The work reported here has been supported by the Maria Curie - Skłodowska University and the National Science Centre (NCN) grant DEC-2017/27/B/ST3/01911 (Poland).

Acknowledgments: I would like to thank James Annett, Grzegorz Litak, and Martin Gradhand for collaboration on some problems tackled in this paper.

Conflicts of Interest: The author declares no conflict of interest.

References

1. Bednorz, J.G.; Müller, K.A. Possible high- T_c superconductivity in the Ba-La-Cu-O system. *Z. Phys. B* **1986**, *64*, 189–193. [[CrossRef](#)]
2. Steglich, F.; Aarts, J.; Bredl, C.D.; Lieke, W.; Meschede, D.; Franz, W.; Schäfer, H. Superconductivity in the presence of strong Pauli paramagnetism: CeCu_2Si_2 . *Phys. Rev. Lett.* **1979**, *43*, 1892–1896. [[CrossRef](#)]
3. Ott, H.R.; Rudigier, H.; Fisk, Z.; Smith, J.L. UBe_{13} : An Unconventional Actinide Superconductor. *Phys. Rev. Lett.* **1983**, *50*, 1595–1598. [[CrossRef](#)]
4. Stewart, G.R.; Fisk, Z.; Willis, J.O.; Smith, J.L. Possibility of existence of bulk superconductivity and spin fluctuations in UPt_3 . *Phys. Rev. Lett.* **1984**, *50*, 679–682. [[CrossRef](#)]
5. Nagamatsu, J.; Nakagawa, N.; Muranaka, T.; Zenitani, Y.; Akimitsu, J. Superconductivity at 39 K in magnesium diboride. *Nature* **2001**, *410*, 63–64. [[CrossRef](#)] [[PubMed](#)]
6. Maeno, Y.; Hashimoto, H.; Yoshida, K.; Nishizaki, S.; Fujita, T.; Bednorz, J.G.; Lichtenberg, F. Superconductivity in a layered perovskite without copper. *Nature* **1994**, *372*, 532–534. [[CrossRef](#)]
7. Drozdov, A.P.; Eremets, M.I.; Troyan, I.A.; Ksenofontov, V.; Shylin, S.I. Conventional superconductivity at 203 kelvin at high pressures in the sulfur hydride system. *Nature* **2015**, *525*, 73–76. [[CrossRef](#)] [[PubMed](#)]
8. Somayazulu, M.; Ahart, M.; Mishra, A.K.; Geballe, Z.M.; Baldini, M.; Meng, Y.; Struzhkin, V.V.; Hemley, R.J. Evidence for Superconductivity above 260 K in Lanthanum Superhydride at Megabar Pressures. *Phys. Rev. Lett.* **2019**, *122*, 027001. [[CrossRef](#)]
9. Gor'kov, L.P. Exotic superconductors. *Phys. Scr.* **1985**, *32*, 6–10. [[CrossRef](#)]
10. Brandow, B. Characteristic features of the exotic superconductors. *Phys. Rep.* **1998**, *296*, 2–63. [[CrossRef](#)]
11. Stewart, G.R. Unconventional superconductivity. *Adv. Phys.* **2017**, *66*, 75–196. [[CrossRef](#)]
12. Kallin, C.; Berlinsky, J. Chiral superconductors. *Rep. Prog. Phys.* **2016**, *79*, 054502. [[CrossRef](#)]
13. Ivanov, D.A. Non-Abelian Statistics of Half-Quantum Vortices in p-Wave Superconductors. *Phys. Rev. Lett.* **2001**, *86*, 268–271. [[CrossRef](#)]

14. Alicea, J. New directions in the pursuit of Majorana fermions in solid state systems. *Rep. Prog. Phys.* **2012**, *75*, 076501. [[CrossRef](#)]
15. Aasen, D.; Hell, M.; Mishmash, R.V.; Andrew Higginbotham, A.; Jeroen Danon, J.; Leijnse, M.; Jespersen, T.S.; Folk, J.A.; Marcus, C.M.; Flensberg, K.; et al. Milestones Toward Majorana-Based Quantum Computing. *Phys. Rev. X* **2016**, *6*, 031016. [[CrossRef](#)]
16. Taylor, E.; Kallin, C. Intrinsic Hall Effect in a Multiband Chiral Superconductor in the Absence of an External Magnetic Field. *Phys. Rev. Lett.* **2012**, *108*, 157001. [[CrossRef](#)]
17. Wysokiński, K.I.; Annett, J.F.; Györfy, B.L. Intrinsic Optical Dichroism in the Chiral Superconducting State of Sr_2RuO_4 . *Phys. Rev. Lett.* **2012**, *108*, 077004. [[CrossRef](#)]
18. Bae, S.; Tan, Y.; Zhuravel, A.P.; Zhang, L.; Zeng, S.; Liu, Y.; Lograsso, T.A.; Prozorov, R.; Venkatesan, A.T.; Anlage, S.M. Dielectric Resonator Method for Determining Gap Symmetry of Superconductors through Anisotropic Nonlinear Meissner Effect. *arXiv* **2019**, arXiv:1901.08762.
19. Schemm, E.R.; Levenson-Falk, E.M.; Kapitulnik, A. Polar Kerr effect studies of time reversal symmetry breaking states in heavy fermion superconductors. *Phys. C Supercond. Appl.* **2017**, *535*, 13–19. [[CrossRef](#)]
20. Vadimov, V.L.; Mel'nikov, A.S. Laser pulse probe of the chirality of Cooper pairs. *Phys. Rev. B* **2017**, *96*, 184523. [[CrossRef](#)]
21. Yerin, Y.; Omelyanchouk, A.; Drechsler, S.L.; Efremov, D.V.; van den Brink, J. Anomalous diamagnetic response in multiband superconductors with broken time-reversal symmetry. *Phys. Rev. B* **2017**, *96*, 144513. [[CrossRef](#)]
22. Gong, X.; Kargarian, M.; Stern, A.; Yue, D.; Zhou, H.; Jin, X.; Galitski, V.M.; Yakovenko, V.M.; Xia, J. Time-reversal symmetry-breaking superconductivity in epitaxial bismuth/nickel bilayers. *Sci. Adv.* **2017**, *3*, e1602579. [[CrossRef](#)] [[PubMed](#)]
23. Chauhan, P.; Mahmood, F.; Yue, D.; Xu, P.C.; Jin, X.; Armitage, N.P. Nodeless Bulk Superconductivity in the Time-Reversal Symmetry Breaking Bi/Ni Bilayer System. *Phys. Rev. Lett.* **2019**, *122*, 017002. [[CrossRef](#)] [[PubMed](#)]
24. Xia, J.; Schemm, E.; Deutscher, G.; Kivelson, S.A.; Bonn, D.A.; Hardy, W.N.; Liang, R.; Siemons, W.; Koster, G.; Fejer, M.M.; et al. Polar Kerr-Effect Measurements of the High-Temperature $\text{YBa}_2\text{Cu}_3\text{O}_{6+x}$ Superconductor: Evidence for Broken Symmetry near the Pseudogap Temperature. *Phys. Rev. Lett.* **2008**, *100*, 127002. [[CrossRef](#)]
25. Sidis, Y.; Ulrich, C.; Bourges, P.; Bernhard, C.; Niedermayer, C.; Regnault, L.P.; Andersen, N.H.; Keimer, B. Antiferromagnetic Ordering in Superconducting $\text{YBa}_2\text{Cu}_3\text{O}_{6.5}$. *Phys. Rev. Lett.* **2001**, *86*, 4100–4103. [[CrossRef](#)]
26. Mook, H.A.; Sidis, Y.; Fauque, B.; Baledent, V.; Bourges, P. Observation of magnetic order in a superconducting $\text{YBa}_2\text{Cu}_3\text{O}_{6.6}$ single crystal using polarized neutron scattering. *Phys. Rev. B* **2008**, 020506. [[CrossRef](#)]
27. Zhang, J.; Ding, Z.; Tan, C.; Huang, K.; Bernal, O.O.; Ho, P.C.; Morris, G.D.; Hillier, A.D.; Biswas, P.K.; Cottrell, S.P.; et al. Discovery of slow magnetic fluctuations and critical slowing down in the pseudogap phase of $\text{YBa}_2\text{Cu}_3\text{O}_y$. *Sci. Adv.* **2018**, *4*, eaao5235. [[CrossRef](#)]
28. Garaud, J.; Silaev, M.; Babaev, E. Thermoelectric Signatures of Time-Reversal Symmetry Breaking States in Multiband Superconductors. *Phys. Rev. Lett.* **2016**, *116*, 097002. [[CrossRef](#)]
29. Ginzburg, V.L. On thermoelectric phenomena in superconductors. *J. Phys. USSR* **1944**, *8*, 148.
30. Van Harlingen, D.J.; Heidel, D.F.; Garland, J.C. Experimental study of thermo-electricity in superconducting indium. *Phys. Rev. B* **1980**, *21*, 1843–1857. [[CrossRef](#)]
31. Barybin, A.A. A Fermi liquid approach to an explanation of the thermoelectric effects experimentally observed in superconductors. *Supercond. Sci. Technol.* **2008**, *21*, 105005. [[CrossRef](#)]
32. Shelly, C.D.; Matrozkova, E.A.; Petrashov, V.T. Resolving thermoelectric “paradox” in superconductors. *Sci. Adv.* **2016**, *2*, e1501250. [[CrossRef](#)]
33. Wysokiński, M.M. Thermoelectric Effect in the Normal Conductor-Superconductor Junction: A BTK Approach. *Acta Phys. Pol. A* **2012**, *122*, 758–764. doi:10.12693/APhysPolA.122.758. [[CrossRef](#)]
34. Wysokiński, M.M.; Spalek, J. Seebeck effect in the graphene-superconductor junction. *J. Appl. Phys.* **2013**, *113*, 163905. [[CrossRef](#)]
35. Amato, A. Heavy-fermion systems studied by μSR technique. *Rev. Mod. Phys.* **1997**, *69*, 1119–1179. [[CrossRef](#)]

36. Sonier, J.E.; Brewer, J.H.; Kiefl, R.F. μ SR studies of the vortex state in type-II superconductors. *Rev. Mod. Phys.* **2000**, *72*, 769–811. [[CrossRef](#)]
37. Hillier, A.D.; Quintanilla, J.; Cywinski, R. Evidence for Time-Reversal Symmetry Breaking in the Noncentrosymmetric Superconductor LaNiC₂. *Phys. Rev. Lett.* **2009**, *102*, 117007. [[CrossRef](#)]
38. Bhattacharyya, A.; Adroja, D.T.; Smidman, M.; Anand, V.K. A brief review on μ SR studies of unconventional Fe- and Cr-based superconductors. *Sci. China-Phys. Mech. Astron.* **2018**, *61*, 127402. [[CrossRef](#)]
39. Capelle, K.; Gross, E.K.U.; Gyorffy, B.L. Theory of dichroism in the electromagnetic response of superconductors. *Phys. Rev. Lett.* **1997**, *78*, 3753–3756. [[CrossRef](#)]
40. Capelle, K.; Gross, E.K.U.; Gyorffy, B.L. Analysis of dichroism in the electromagnetic response of superconductors. *Phys. Rev. B* **1998**, *58*, 473–489. [[CrossRef](#)]
41. White, R.M.; Geballe, T.H. *Long Range Order in Solids*; Academic: New York, NY, USA, 1979; pp. 317–321.
42. Lutchyn, R.M.; Nagornykh, P.; Yakovenko, V.M. Gauge-invariant electromagnetic response of a chiral $p_x + ip_y$ superconductor. *Phys. Rev. B* **2008**, *77*, 144516. [[CrossRef](#)]
43. Kapitulnik, A.; Xia, J.; Schemm, E.; Palevski, A. Polar Kerr effect as probe for time-reversal symmetry breaking in unconventional superconductors. *New J. Phys.* **2009**, *11*, 055060. [[CrossRef](#)]
44. Kapitulnik, A. Notes on constraints for the observation of Polar Kerr Effect in complex materials. *Physica B* **2015**, *460*, 151–158. [[CrossRef](#)]
45. Tokura, Y.; Nagaosa, N. Nonreciprocal responses from noncentrosymmetric quantum materials. *Nat. Commun.* **2018**, *9*, 3740. [[CrossRef](#)]
46. Annett, J.F.; Gyorffy, B.L.; Wysokiński, K.I. Orbital magnetic moment of a chiral p-wave superconductor. *New J. Phys.* **2009**, *11*, 055063. [[CrossRef](#)]
47. Schlabbitz, W.; Baumann, J.; Pollit, B.; Rauchschalbe, U.; Mayer, H.M.; Ahlheim, U.; Bredl, C.D. Superconductivity and magnetic order in a strongly interacting fermi-system: URu₂Si₂. *Z. Phys. B* **2015**, *62*, 171–177. [[CrossRef](#)]
48. Mydosh, J.A.; Oppeneer, P.M. *Colloquium: Hidden order, superconductivity, and magnetism: The unsolved case of URu₂Si₂*. *Rev. Mod. Phys.* **2011**, *83*, 1301–1322. [[CrossRef](#)]
49. Luke, G.M.; Keren, A.; Le, L.P.; Wu, W.D.; Uemura, Y.J.; Bonn, D.A.; Taillefer, L.; Garrett, J.D. Muon spin relaxation in UPt₃. *Phys. Rev. Lett.* **1993**, *71*, 1466–1469. [[CrossRef](#)]
50. Brawner, D.A.; Ott, H.R.; Fisk, Z. Further evidence for time reversal symmetry breaking in the heavy electron superconductor UPt₃. *Phys. B Condens. Matter* **1997**, 230–232, 338–341. [[CrossRef](#)]
51. Joynt, R.; Taillefer, L. The superconducting phases of UPt₃. *Rev. Mod. Phys.* **2002**, *74*, 235–294. [[CrossRef](#)]
52. Adenwalla, S.; Lin, S.W.; Ran, Q.Z.; Zhao, Z.; Ketterson, J.B.; Sauls, J.A.; Taillefer, L.; Hinks, D.G.; Levy, M.; Sarma, B.K. Phase diagram of UPt₃ from ultrasonic velocity measurements. *Phys. Rev. Lett.* **1990**, *65*, 2298–2301. [[CrossRef](#)] [[PubMed](#)]
53. Shu, L.; Higemoto, W.; Aoki, Y.; Hillier, A.D.; Ohishi, K.; Ishida, K.; Kadono, R.; Koda, A.; Bernal, O.O.; MacLaughlin, D.E.; et al. Suppression of time-reversal symmetry breaking superconductivity in Pr(Os_{1-x}Ru_x)₄Sb₁₂ and Pr_{1-y}La_yOs₄Sb₁₂. *Phys. Rev. B* **2011**, *83*, 100504. [[CrossRef](#)]
54. Luke, G.M.; Fudamoto, Y.; Kojima, K.M.; Larkin, M.I.; Merrin, J.; Nachumi, B.; Uemura, Y.J.; Maeno, Y.; Mao, Z.Q.; Mori, Y.; et al. Time reversal symmetry-breaking superconductivity in Sr₂RuO₄. *Nature* **1998**, *394*, 558–561. [[CrossRef](#)]
55. Xia, J.; Maeno, Y.; Beyersdorf, P.T.; Fejer, M.M.; Kapitulnik, A. High resolution polar Kerr effect measurements of Sr₂RuO₄: Evidence for broken time-reversal symmetry in the superconducting state. *Phys. Rev. Lett.* **2006**, *97*, 167002. [[CrossRef](#)]
56. Schemm, E.R.; Gannon, W.J.; Wishne, C.M.; Halperin, W.P.; Kapitulnik, A. Observation of broken time-reversal symmetry in the heavy-fermion superconductor UPt₃. *Science* **2014**, *345*, 190–193. [[CrossRef](#)] [[PubMed](#)]
57. Schemm, E.R.; Baumbach, R.E.; Tobash, P.H.; Ronning, F.; Bauer, E.D.; Kapitulnik, A. Evidence for broken time-reversal symmetry in the superconducting phase of URu₂Si₂. *Phys. Rev. B* **2015**, *91*, 140506. [[CrossRef](#)]
58. Aoki, Y.; Tsuchiya, A.; Kanayama, T.; Saha, S.R.; Sugawara, H.; Sato, H.; Higemoto, W.; Koda, A.; Ohishi, K.; Nishiyama, K.; et al. Time-Reversal Symmetry-Breaking Superconductivity in Heavy-Fermion PrOs₄Sb₁₂ Detected by Muon-Spin Relaxation. *Phys. Rev. Lett.* **2003**, *91*, 067003. [[CrossRef](#)] [[PubMed](#)]

59. Levenson-Falk, E.M.; Schemm, E.R.; Aoki, Y.; Maple, M.B.; Kapitulnik, A. Polar Kerr Effect from Time-Reversal Symmetry Breaking in the Heavy-Fermion Superconductor PrOs₄Sb₁₂. *Phys. Rev. Lett.* **2018**, *120*, 187004. [[CrossRef](#)] [[PubMed](#)]
60. Bauer, E.D.; Frederick, N.A.; Ho, P.-C.; Zapf, V.S.; Maple, M.B. Superconductivity and heavy fermion behavior in PrOs₄Sb₁₂. *Phys. Rev. B* **2002**, *65*, 100506. [[CrossRef](#)]
61. Maisuradze, A.; Schnelle, W.; Khasanov, R.; Gumeniuk, R.; Nicklas, M.; Rosner, H.; Leithe-Jasper, A.; Grin, Y.; Amato, A.; Thalmeier, P. Evidence for time-reversal symmetry breaking in superconducting PrPt₄Ge₁₂. *Phys. Rev. B* **2010**, *82*, 024524. [[CrossRef](#)]
62. Grinenko, V.; Materne, P.; Sarkar, R.; Luetkens, H.; Kihou, K.; Lee, C.H.; Akhmadaliev, S.; Efremov, D.V.; Drechsler, S.L.; Klauss, H.H. Superconductivity with broken time-reversal symmetry in ion-irradiated Ba_{0.27}K_{0.73}Fe₂As₂ single crystals. *Phys. Rev. B* **2017**, *95*, 214511. [[CrossRef](#)]
63. Hillier, A.D.; Quintanilla, J.; Mazidian, B.; Annett, J.F.; Cywinski, R. Nonunitary Triplet Pairing in the Centrosymmetric Superconductor LaNiGa₂. *Phys. Rev. Lett.* **2012**, *109*, 097001. [[CrossRef](#)] [[PubMed](#)]
64. Shang, T.; Pang, G.M.; Baines, C.; Jiang, W.B.; Xie, W.; Wang, A.; Medarde, M.; Pomjakushina, E.; Shi, M.; Mesot, J.; et al. Nodeless superconductivity and time-reversal symmetry breaking in the noncentrosymmetric superconductor Re₂₄Ti₅. *Phys. Rev. B* **2018**, *97*, 020502. [[CrossRef](#)]
65. Biswas, P.K.; Luetkens, H.; Neupert, T.; Stürzer, T.; Baines, C.; Pascua, G.; Schnyder, A.P.; Fischer, M.H.; Goryo, J.; Lees, M.R.; et al. Evidence for superconductivity with broken time-reversal symmetry in locally noncentrosymmetric SrPtAs. *Phys. Rev. B* **2013**, *87*, 180503. [[CrossRef](#)]
66. Quintanilla, J.; Hillier, A.D.; Annett, J.F.; Cywinski, R. Relativistic analysis of the pairing symmetry of the noncentrosymmetric superconductor LaNiC₂. *Phys. Rev. B* **2010**, *82*, 174511. [[CrossRef](#)]
67. Bhattacharyya, A.; Adroja, D.T.; Quintanilla, J.; Hillier, A.D.; Kase, N.; Strydom, A.M.; Akimitsu, J. Broken time-reversal symmetry probed by muon spin relaxation in the caged type superconductor Lu₅Rh₆Sn₁₈. *Phys. Rev. B* **2015**, *91*, 060503. [[CrossRef](#)]
68. Barker, J.A.T.; Singh, D.; Thamizhavel, A.; Hillier, A.D.; Less, M.R.; Balakrishnan, G.; Paul, D.; Singh, R.P. Unconventional Superconductivity in La₇Ir₃ Revealed by Muon Spin Relaxation: Introducing a New Family of Noncentrosymmetric Superconductor That Breaks Time-Reversal Symmetry. *Phys. Rev. Lett.* **2015**, *115*, 267001. [[CrossRef](#)] [[PubMed](#)]
69. Singh, D.; Scheurer, M.S.; Hillier, A.D.; Singh, R.P. Time reversal symmetry breaking and unconventional pairing in the noncentrosymmetric superconductor La₇Rh₃ probed by μ SR. *arXiv* **2018**, arXiv:1802.01533.
70. Singh, R.P.; Hillier, A.D.; Mazidian, B.; Quintanilla, J.; Annett, J.F.; Paul, D.; Balakrishnan, G.; Lees, M.R. Detection of time-reversal symmetry breaking in the noncentrosymmetric superconductor Re₆Zr using muon-spin spectroscopy. *Phys. Rev. Lett.* **2014**, *112*, 107002. [[CrossRef](#)] [[PubMed](#)]
71. Pang, G.M.; Nie, Z.Y.; Wang, A.; Singh, D.; Xie, W.; Jiang, W.B.; Chen, Y.; Singh, R.P.; Smidman, M.; Yuan, H.Q. Fully gapped superconductivity in single crystals of noncentrosymmetric Re₆Zr with broken time-reversal symmetry. *Phys. Rev. B* **2018**, *97*, 224506. [[CrossRef](#)]
72. Singh, D.; Barker, J.A.T.; Thamizhavel, A.; Paul, D.; Hillier, A.D.; Singh, R.P. Time-reversal symmetry breaking in the noncentrosymmetric superconductor Re₆Hf: Further evidence for unconventional behavior in the α -Mn family of materials. *Phys. Rev. B* **2017**, *96*, 180501. [[CrossRef](#)]
73. Singh, D.; Sajilesh, K.P.; Barker, J.A.T.; Paul, D.M.K.; Hillier, A.D.; Singh, R.P. Time reversal symmetry breaking in noncentrosymmetric superconductor Re₆Ti. *Phys. Rev. B* **2018**, *97*, 100505. [[CrossRef](#)]
74. Shang, T.; Ghosh, S.K.; Chang, L.-J.; Baines, C.; Lee, M.K.; Zhao, J.Z.; Verezhak, J.A.T.; Gawryluk, D.J.; Pomjakushina, E.; Shi, M.; et al. Time-reversal symmetry breaking and unconventional superconductivity in Zr₃Ir: A new type of noncentrosymmetric superconductor. *arXiv* **2019**, arXiv:1901.01414.
75. Zhang, J.; MacLaughlin, D.E.; Hillier, A.D.; Ding, Z.F.; Huang, K.; Maple, M.B.; Shu, L. Broken time-reversal symmetry in superconducting Pr_{1-x}Ce_xPt₄Ge₁₂. *Phys. Rev. B* **2015**, *91*, 104523. [[CrossRef](#)]
76. Shang, T.; Gawryluk, D.J.; Verezhak, J.A.T.; Pomjakushina, E.; Shi, M.; Medarde, M.; Mesot, J.; Shiroka, T. Structure and superconductivity in the binary Re_{1-x}Mo_x alloys. *Phys. Rev. Mater.* **2019**, *3*, 024801. [[CrossRef](#)]
77. Smidman, M.; Salamon, M.B.; Yuan, H.Q.; Agterberg, D.F. Superconductivity and spin-orbit coupling in non-centrosymmetric materials: A review. *Rep. Progr. Phys.* **2017**, *80*, 036501. [[CrossRef](#)]
78. Mackenzie, A.P.; Scaffidi, T.; Hicks, C.W.; Maeno, Y. Even odder after twenty-three years: the superconducting order parameter puzzle of Sr₂RuO₄. *NPJ Quantum Mater.* **2017**, *2*, 40. [[CrossRef](#)]

79. Pchelkina, Z.V.; Nekrasov, I.A.; Pruschke, T.; Sekiyama, A.; Suga, S.; Anisimov, V.I.; Vollhardt, D. Evidence for strong electronic correlations in the spectra of Sr₂RuO₄. *Phys. Rev. B* **2007**, *75*, 035122. [[CrossRef](#)]
80. Rozbicki, E.J.; Annett, J.F.; Souquet, J.-R.; Mackenzie, A.P. Spin-orbit coupling and k-dependent Zeeman splitting in strontium ruthenate. *J. Phys. Condens. Matter* **2011**, *23*, 094201. [[CrossRef](#)]
81. Haverkort, M.W.; Elfimov, I.S.; Tjeng, L.H.; Sawatzky, G.A.; Damascelli, A. Strong Spin-Orbit Coupling Effects on the Fermi Surface of Sr₂RuO₄ and Sr₂RhO₄. *Phys. Rev. Lett.* **2008**, *101*, 026406. [[CrossRef](#)]
82. Facio, J.I.; Mravljje, J.; Pourovskii, L.; Cornaglia, P.S.; Vildosola, V. Spin-orbit and anisotropic strain effects on the electronic correlations in Sr₂RuO₄. *Phys. Rev. B* **2018**, *98*, 085121. [[CrossRef](#)]
83. Mackenzie, A.P.; Maeno, Y. The superconductivity of Sr₂RuO₄ and the physics of spin-triplet pairing. *Rev. Mod. Phys.* **2003**, *75*, 657–712. [[CrossRef](#)]
84. Kallin, C. Chiral p-wave order in Sr₂RuO₄. *Rep. Prog. Phys.* **2012**, *75*, 042501. [[CrossRef](#)]
85. Maeno, Y.; Kittaka, S.; Nomura, T.; Yonezawa, S.; Ishida, K. Evaluation of Spin-Triplet Superconductivity in Sr₂RuO₄. *J. Phys. Soc. Jpn.* **2012**, *81*, 011009. [[CrossRef](#)]
86. Lichtenberg, F. The story of Sr₂RuO₄. *Prog. Solid State Chem.* **2002**, *30*, 103–131. [[CrossRef](#)]
87. Hussey, N.E.; Mackenzie, A.P.; Cooper, J.R.; Maeno, Y.; Nishizaki, S.; Fujita, T. Normal-state magnetoresistance of Sr₂RuO₄. *Phys. Rev. B* **1998**, *57*, 5505–5511. [[CrossRef](#)]
88. Mackenzie, A.P.; Haselwimmer, R.K.W.; Tyler, A.W.; Lonzarich, G.G.; Mori, Y.; Nishizaki, S.; Maeno, Y. Extremely Strong Dependence of Superconductivity on Disorder in Sr₂RuO₄. *Phys. Rev. Lett.* **1998**, *80*, 161–164. [[CrossRef](#)]
89. Agterberg, D.F.; Rice, T.M.; Sigrist, M. Orbital dependent superconductivity in Sr₂RuO₄. *Phys. Rev. Lett.* **1997**, *78*, 3374–3377. [[CrossRef](#)]
90. Zhitomirsky, M.E.; Rice, T.M. Interband proximity effect and nodes of superconducting gap in Sr₂RuO₄. *Phys. Rev. Lett.* **2001**, *87*, 057001. [[CrossRef](#)]
91. Konik, R.M.; Rice, T.M. Orbital dependence of quasiparticle lifetimes in Sr₂RuO₄. *Phys. Rev. B* **2007**, *76*, 104501. [[CrossRef](#)]
92. Zegrodnik, M.; Bünemann, J.; Spalek, J. Even-parity spin-triplet pairing by purely repulsive interactions for orbitally degenerate correlated fermions. *New J. Phys.* **2014**, *16*, 033001. [[CrossRef](#)]
93. Wysockiński, M.M.; Kaczmarczyk, J.; Spalek, J. Correlation-driven d-wave superconductivity in Anderson lattice model: Two gaps. *Phys. Rev. B* **2016**, *94*, 024517. [[CrossRef](#)]
94. Aoki, D.; Ishida, K.; Flouquet, J. Review of U-based Ferromagnetic Superconductors: Comparison between UGe₂, URhGe, and UCoGe. *J. Phys. Soc. Jpn.* **2019**, *88*, 022001. [[CrossRef](#)]
95. Raghu, S.; Kapitulnik, A.; Kivelson, S.A. Hidden Quasi-One-Dimensional Superconductivity in Sr₂RuO₄. *Phys. Rev. Lett.* **2010**, *105*, 136401. [[CrossRef](#)]
96. Wang, Q.H.; Platt, C.; Yang, Y.; Honerkamp, C.; Zhang, F.C.; Hanke, W.; Rice, T.M.; Thomale, R. Theory of superconductivity in a three-orbital model of Sr₂RuO₄. *EPL Europhys. Lett.* **2013**, *104*, 17013. [[CrossRef](#)]
97. Gao, Y.; Zhou, T.; Huang, H.; Ting, C.S.; Tong, P.; Wang, Q.-H. Probing active/passive bands by quasiparticle interference in Sr₂RuO₄. *Phys. Rev. B* **2013**, *88*, 094514. [[CrossRef](#)]
98. Akebi, S.; Kondo, T.; Nakayama, M.; Kuroda, K.; Kunisada, S.; Taniguchi, H.; Maeno, Y.; Shin, S. Low-energy electron-mode couplings in the surface bands of Sr₂RuO₄ revealed by laser-based angle-resolved photoemission spectroscopy. *Phys. Rev. B* **2019**, *99*, 081108. [[CrossRef](#)]
99. Rice, T.M.; Sigrist, M. Sr₂RuO₄: An electronic analogue of ³He?. *J. Phys. Condens. Matter* **1995**, *7*, L643–L648. [[CrossRef](#)]
100. Mazin, I.I.; Singh, D.J. Ferromagnetic spin fluctuation induced superconductivity in Sr₂RuO₄. *Phys. Rev. Lett.* **1997**, *79*, 733–736. [[CrossRef](#)]
101. Sidis, Y.; Braden, M.; Bourges, P.; Hennion, B.; Nishizaki, S.; Maeno, Y.; Mori, Y. Evidence for Incommensurate Spin Fluctuations in Sr₂RuO₄. *Phys. Rev. Lett.* **1999**, *83*, 3320–3323. [[CrossRef](#)]
102. Braden, M.; Sidis, Y.; Bourges, P.; Pfeuty, P.; Kulda, J.; Mao, Z.; Maeno, Y. Inelastic neutron scattering study of magnetic excitations in Sr₂RuO₄. *Phys. Rev. B* **2002**, *66*, 064522. [[CrossRef](#)]
103. Braden, M.; Steffens, P.; Sidis, Y.; Kulda, J.; Bourges, P.; Hayden, S.; Kikugawa, N.; Maeno, Y. Anisotropy of the Incommensurate Fluctuations in Sr₂RuO₄: A Study with Polarized Neutrons. *Phys. Rev. Lett.* **2004**, *92*, 097402. [[CrossRef](#)]

104. Iida, K.; Kofu, M.; Katayama, N.; Lee, J.; Kajimoto, R.; Inamura, Y.; Nakamura, M.; Arai, M.; Yoshida, Y.; Fujita, M.; et al. Inelastic neutron scattering study of the magnetic fluctuations in Sr₂RuO₄. *Phys. Rev. B* **2011**, *84*, 060402. [[CrossRef](#)]
105. Ortmann, J.E.; Liu, J.Y.; Hu, J.; Zhu, M.; Peng, J.; Matsuda, M.; Ke, X.; Mao, Z.Q. Competition Between Antiferromagnetism and Ferromagnetism in Sr₂RuO₄ Probed by Mn and Co Doping. *Sci. Rep.* **2013**, *3*, 2950. [[CrossRef](#)]
106. Steffens, P.; Sidis, Y.; Kulda, J.; Mao, Z.Q.; Maeno, Y.; Mazin, I.I.; Braden, M. Spin Fluctuations in Sr₂RuO₄ from Polarized Neutron Scattering: Implications for Superconductivity. *Phys. Rev. Lett.* **2019**, *122*, 047004. [[CrossRef](#)]
107. Annett, J.F.; Litak, G.; Gyorffy, B.L.; Wysokiński, K.I. Interlayer coupling and p-wave pairing in strontium ruthenate. *Phys. Rev. B* **2002**, *66*, 134514. [[CrossRef](#)]
108. Annett, J.F.; Gyorffy, B.L.; Litak, G.; Wysokiński, K.I. Gap nodes and time reversal symmetry breaking in strontium ruthenate. *Eur. Phys. J. B* **2003**, *36*, 301–312. [[CrossRef](#)]
109. Wysokiński, K.I.; Litak, G.; Annett, J.F.; Gyorffy, B.L. Spin triplet superconductivity in Sr₂RuO₄. *Phys. Status Solidi B* **2003**, *236*, 325–331. [[CrossRef](#)]
110. Annett, J.F.; Litak, G.; Gyorffy, B.L.; Wysokiński, K.I. Spin-orbit coupling and symmetry of the order parameter in strontium ruthenate. *Phys. Rev. B* **2006**, *73*, 134501. [[CrossRef](#)]
111. Wysokiński, K.I.; Annett, J.F.; Gyorffy, B.L. Orbital-dependent pairing effects in the nuclear spin-lattice relaxation rate of Sr₂RuO₄. *Supercond. Sci. Technol.* **2009**, *22*, 014009. [[CrossRef](#)]
112. Mackenzie, A.P.; Julian, S.R.; Diver, A.J.; McMullan, G.J.; Ray, M.P.; Lonzarich, G.G.; Maeno, Y.; Nishizaki, S.; Fujita, T. Quantum Oscillations in the Layered Perovskite Superconductor Sr₂RuO₄. *Phys. Rev. Lett.* **1996**, *76*, 3786–3789. [[CrossRef](#)]
113. Bergemann, C.; Julian, S.R.; Mackenzie, A.P.; NishiZaki, S.; Maeno, Y. Detailed Topography of the Fermi Surface of Sr₂RuO₄. *Phys. Rev. Lett.* **2000**, *84*, 2662–2665. [[CrossRef](#)]
114. Leggett, A.J. A theoretical description of the new phases of liquid ³He. *Rev. Mod. Phys.* **1975**, *47*, 331–414. [[CrossRef](#)]
115. Annett, J.F. Symmetry of the order parameter for high-temperature superconductivity. *Adv. Phys.* **1990**, *39*, 83–126. [[CrossRef](#)]
116. Ishida, K.; Mukuda, H.; Kitaoka, Y.; Asayama, K.; Mao, Z.Q.; Mori, Y.; Maeno, Y. Spin-triplet superconductivity in Sr₂RuO₄ identified by ¹⁷O Knight shift. *Nature* **1998**, *396*, 658–660. [[CrossRef](#)]
117. Duffy, J.A.; Hayden, S.M.; Maeno, Y.; Mao, Z.; Kulda, J.; McIntyre, J. Polarized-Neutron Scattering Study of the Cooper-Pair Moment in Sr₂RuO₄. *Phys. Rev. Lett.* **2000**, *85*, 5412–5415. [[CrossRef](#)]
118. Murakawa, H.; Ishida, K.; Kitagawa, K.; Mao, Z.Q.; Maeno, Y. Measurement of the ¹⁰¹Ru-Knight Shift of Superconducting Sr₂RuO₄ in a Parallel Magnetic Field. *Phys. Rev. Lett.* **2004**, *93*, 167004. [[CrossRef](#)]
119. Annett, J.F.; Györffy, B.L.; Litak, G.; Wysokiński, K. Magnetic field induced rotation of the d-vector in the spin-triplet superconductor Sr₂RuO₄. *Phys. Rev. B* **2008**, *78*, 054511. [[CrossRef](#)]
120. Annett, J.F.; Litak, G.; Gyorffy, B.L.; Wysokiński, K.I. Magnetic field induced rotation of the d-vector in Sr₂RuO₄. *Phys. C Supercond.* **2007**, *460–462*, 995–996. [[CrossRef](#)]
121. Kuhn, S.J.; Morgenlander, W.; Loudon, E.R.; Rastovski, C.; Gannon, W.J.; Takatsu, H.; Peets, D.C.; Maeno, Y.; Dewhurst, C.D.; Gavilano, J.; et al. Anisotropy and multiband superconductivity in Sr₂RuO₄ determined by small-angle neutron scattering studies of the vortex lattice. *Phys. Rev. B* **2017**, *96*, 174507. [[CrossRef](#)]
122. Kittaka, S.; Kasahara, A.; Sakakibara, T.; Shibata, D.; Yonezawa, S.; Maeno, Y.; Tenya, K.; Machida, K. Sharp magnetization jump at the first-order superconducting transition in Sr₂RuO₄. *Phys. Rev. B* **2014**, *90*, 220502. [[CrossRef](#)]
123. Dodaro, J.F.; Wang, Z.; Kallin, C. Effects of deep superconducting gap minima and disorder on residual thermal transport in Sr₂RuO₄. *Phys. Rev. B* **2018**, *98*, 214520. [[CrossRef](#)]
124. Hassinger, E.; Bourgeois-Hope, P.; Taniguchi, H.; René de Cotret, S.; Grissonnanche, G.; Anwar, M.S.; Maeno, Y.; Doiron-Leyraud, N.; Taillefer, L. Vertical Line Nodes in the Superconducting Gap Structure of Sr₂RuO₄. *Phys. Rev. X* **2017**, *7*, 011032. [[CrossRef](#)]
125. Yarzhemsky, V.G. Group Theoretical Lines of Nodes in Triplet Chiral Superconductor Sr₂RuO₄. *J. Phys. Soc. Jpn.* **2018**, *87*, 114711. [[CrossRef](#)]
126. Sigrist, M.; Ueda, K. Phenomenological theory of unconventional superconductivity. *Rev. Mod. Phys.* **1991**, *63*, 239–311. [[CrossRef](#)]

127. Kirtley, J.R.; Kallin, C.; Hicks, C.W.; Kim, E.-A.; Liu, Y.; Moler, K.A.; Maeno, Y.; Nelson, K.D. Upper limit on spontaneous supercurrents in Sr₂RuO₄. *Phys. Rev. B* **2007**, *76*, 014526. [[CrossRef](#)]
128. Hicks, C.W.; Kirtley, J.R.; Lippman, T.M.; Koshnick, N.C.; Huber, M.E.; Maeno, Y.; Yuhasz, W.M.; Maple, M.B.; Moler, K.A. Limits on superconductivity-related magnetization in Sr₂RuO₄ and PrOs₄Sb₁₂ from scanning SQUID microscopy. *Phys. Rev. B* **2010**, *81*, 214501. [[CrossRef](#)]
129. Curran, P.J.; Bending, S.J.; Desoky, W.M.; Gibbs, A.S.; Lee, S.L.; Mackenzie, A.P. Search for spontaneous edge currents and vortex imaging in Sr₂RuO₄ mesostructures. *Phys. Rev. B* **2014**, *89*, 144504. [[CrossRef](#)]
130. Aoki, Y.; Tayama, T.; Sakakibara, T.; Kuwahara, K.; Iwasa, K.; Kohgi, M.; Higemoto, W.; MacLaughlin, D.E.; Sugawara, H.; Sato, H. The Unconventional Superconductivity of Skutterudite PrOs₄Sb₁₂: Time-Reversal Symmetry Breaking and Adjacent Field-Induced Quadrupole Ordering. *J. Phys. Soc. Jpn.* **2007**, *76*, 051006. [[CrossRef](#)]
131. Ashby, P.E.C.; Kallin, C. Suppression of spontaneous supercurrents in a chiral p-wave superconductor. *Phys. Rev. B* **2009**, *79*, 224509. [[CrossRef](#)]
132. Lederer, S.; Huang, W.; Taylor Raghun, E.S.; Kallin, C. Suppression of spontaneous currents in Sr₂RuO₄ by surface disorder. *Phys. Rev. B* **2014**, *90*, 134521. [[CrossRef](#)]
133. Huang, W.; Lederer, S.; Taylor, E.; Kallin, C. Nontopological nature of the edge current in a chiral p-wave superconductor. *Phys. Rev. B* **2015**, *91*, 094507. [[CrossRef](#)]
134. Etter, S.B.; Bouhon, A.; Sigrist, M. Spontaneous surface flux pattern in chiral p-wave superconductors. *Phys. Rev. B* **2018**, *97*, 064510. [[CrossRef](#)]
135. Matsumoto, M.; Sigrist, M. Quasiparticle States near the Surface and the Domain Wall in a $p_x \pm ip_y$ -Wave Superconductor. *J. Phys. Soc. Jpn.* **1999**, *68*, 994–1007. [[CrossRef](#)]
136. Read, N.; Green, D. Paired states of fermions in two dimensions with breaking of parity and time-reversal symmetries and the fractional quantum Hall effect. *Phys. Rev. B* **2000**, *61*, 10267–10297. [[CrossRef](#)]
137. Palacio-Morales, A.; Mascot, E.; Cocklin, S.; Kim, H.; Rachel, S.; Morr, D.K.; Wiesendanger, R. Atomic-Scale Interface Engineering of Majorana Edge Modes in a 2D Magnet-Superconductor Hybrid System. *arXiv* **2019**, arXiv:1809.04503.
138. Mazur, G.P.; Dybko, K.; Szczerbakow, A.; Kazakov, A.; Zgirski, M.; Lusakowska, E.; Kret, S.; Korczak, J.; Story, S.; Sawicki, M.; et al. Experimental search for the origin of zero-energy modes in topological materials. *arXiv* **2019**, arXiv:1709.04000.
139. Brzezicki, W.; Wysokiński, M.; Hyart, T. Topological properties of multilayers and surface steps in the SnTe material class. *arXiv* **2019**, arXiv:1812.02168.
140. Das, S.; Aggarwal, L.; Roychowdhury, S.; Aslam, M.; Gayen, S.; Biswas, K.; Sheet, G. Unexpected superconductivity at nanoscale junctions made on the topological crystalline insulator Pb_{0.6}Sn_{0.4}Te. *Appl. Phys. Lett.* **2016**, *109*, 132601. [[CrossRef](#)]
141. Aggarwal, L.; Gaurav, A.; Thakur, G.S.; Haque, Z.; Ganguli, A.K.; Sheet, G. Unconventional superconductivity at mesoscopic point contacts on the 3D Dirac semimetal Cd₃As₂. *Nat. Mater.* **2016**, *15*, 32–37. [[CrossRef](#)]
142. Awoga, O.A.; Cayao, J.; Annica, M.; Black-Schaffer, A.M. Supercurrent detection of topologically trivial zero-energy states in nanowire junctions. *arXiv* **2019**, arXiv:1904.03783.
143. Lutchyn, R.M.; Nagornykh, P.; Yakovenko, V.M. Frequency and temperature dependence of the anomalous ac Hall conductivity in a chiral $p_x + ip_y$ superconductor with impurities. *Phys. Rev. B* **2009**, *80*, 104508. [[CrossRef](#)]
144. Ebert, H. Magneto-optical effects in transition metal systems. *Rep. Prog. Phys.* **1996**, *59*, 1665–1835. [[CrossRef](#)]
145. Yip, S.K.; Sauls, J.A. Circular dichroism and birefringence in unconventional superconductors. *J. Low Temp. Phys.* **1992**, *86*, 257–290. [[CrossRef](#)]
146. Roy, R.; Kallin, C. Collective modes and electromagnetic response of a chiral superconductor. *Phys. Rev. B* **2008**, *77*, 174513. [[CrossRef](#)]
147. Goryo, J. Impurity-induced polar Kerr effect in a chiral p-wave superconductor. *Phys. Rev. B* **2008**, *78*, 060501. [[CrossRef](#)]
148. Mineev, V.P. Recent developments in unconventional superconductivity. *J. Low Temp. Phys.* **2010**, *158*, 615–630. [[CrossRef](#)]
149. Taylor, E.; Kallin, C. Anomalous Hall conductivity of clean Sr₂RuO₄ at finite temperatures. *J. Phys. Conf. Ser.* **2013**, *449*, 012036. [[CrossRef](#)]

150. Gradhand, M.; Wysokiński, K.I.; Annett, J.F.; Gyiffy, B.L. Kerr rotation in the unconventional superconductor Sr_2RuO_4 . *Phys. Rev. B* **2013**, *88*, 094504. [[CrossRef](#)]
151. Gradhand, M.; Annett, J.F.; Wysokiński, K.I. Three-band intrinsic Kerr effect in Sr_2RuO_4 . *Philos. Mag.* **2015**, *95*, 525–537. [[CrossRef](#)]
152. Wang, Z.; Berlinsky, J.; Zwicknagl, G.; Kallin, C. Intrinsic ac anomalous Hall effect of nonsymmorphic chiral superconductors with an application to UPt_3 . *Phys. Rev. B* **2017**, *96*, 174511. [[CrossRef](#)]
153. Wu, L.; Salehi, M.; Koirala, N.; Moon, J.; Oh, S.; Armitage, N.P. Quantized Faraday and Kerr rotation and axion electrodynamics of a 3D topological insulator. *Science* **2016**, *354*, 1124–1127. [[CrossRef](#)] [[PubMed](#)]
154. König, E.J.; Levchenko, A. Kerr Effect from Diffractive Skew Scattering in Chiral $p_x \pm ip_y$ Superconductors. *Phys. Rev. Lett.* **2017**, *118*, 027001. [[CrossRef](#)]
155. Robbins, J.; Annett, J.F.; Gradhand, M. Effect of spin-orbit coupling on the polar Kerr effect in Sr_2RuO_4 . *Phys. Rev. B* **2017**, *96*, 144503. [[CrossRef](#)]
156. Anwar, M.S.; Ishiguro, R.; Nakamura, T.; Yakabe, M.; Yonezawa, S.; Takayanagi, H.; Maeno, Y. Multicomponent order parameter superconductivity of Sr_2RuO_4 revealed by topological junctions. *Phys. Rev. B* **2017**, *95*, 224509. [[CrossRef](#)]
157. Watson, C.A.; Gibbs, A.S.; Mackenzie, A.P.; Hicks, C.W.; Moler, K.A. Micron-scale measurements of low anisotropic strain response of local Tc in Sr_2RuO_4 . *Phys. Rev. B* **2018**, *98*, 094521. [[CrossRef](#)]
158. Yang, F.; Yu, T.; Wu, M.W. Anomalous Hall effect in semiconductor quantum wells in proximity to chiral p-wave superconductors. *Phys. Rev. B* **2018**, *97*, 205301. [[CrossRef](#)]
159. Huang, W.; Yao, H. Possible Three-Dimensional Nematic Odd-Parity Superconductivity in Sr_2RuO_4 . *Phys. Rev. Lett.* **2018**, *121*, 157002. [[CrossRef](#)]
160. Wang, X.; Wang, Z.; Kallin, C. Spontaneous edge current in higher chirality superconductors. *Phys. Rev. B* **2018**, *98*, 094501. [[CrossRef](#)]
161. Zhang, J.-L.; Huang, W.; Yao, D.-X. Spontaneous surface current in multicomponent cubic superconductors with time-reversal symmetry breaking. *Phys. Rev. B* **2018**, *98*, 014511. [[CrossRef](#)]
162. Wu, Z.; Yan, Z.; Huang, W. Higher-order topological superconductivity: Possible realization in Fermi gases and Sr_2RuO_4 . *Phys. Rev. B* **2019**, *99*, 020508. [[CrossRef](#)]
163. Komendova, L.; Black-Schaffer, A.M. Odd-Frequency Superconductivity in Sr_2RuO_4 Measured by Kerr Rotation. *Phys. Rev. Lett.* **2017**, *119*, 087001. [[CrossRef](#)]
164. Triola, C.; Black-Schaffer, A.M. Odd-frequency pairing and Kerr effect in the heavy-fermion superconductor UPt_3 . *Phys. Rev. B* **2018**, *97*, 064505. [[CrossRef](#)]



© 2019 by the author. Licensee MDPI, Basel, Switzerland. This article is an open access article distributed under the terms and conditions of the Creative Commons Attribution (CC BY) license (<http://creativecommons.org/licenses/by/4.0/>).